Myeloid cell TBK1 restricts inflammatory responses

Tianxiao Gao[a,1,2], Ting Liu[a,2,3], Chun-Jung Ko[a,b,2,4], Lingyun Zhang[a,5], Donghyun Joo[a,6], Xiaoping Xie[a,7], Lele Zhu[a], Yanchuan Li[a], Xuhong Cheng[a], and Shao-Cong Sun[a,c,4]

[a]Department of Immunology, The University of Texas MD Anderson Cancer Center, Houston, TX 77030; [b]Graduate Institute of Immunology, College of Medicine, National Taiwan University, Taipei, Taiwan 100233; and [c]MD Anderson Cancer Center UT Health Graduate School of Biomedical Sciences, Houston, TX 77030

Edited by Katherine Fitzgerald, University of Massachusetts Medical School, Worcester, MA; received April 27, 2021; accepted November 23, 2021

Proinflammatory cytokine production by innate immune cells plays a crucial role in inflammatory diseases, but the molecular mechanisms controlling the inflammatory responses are poorly understood. Here, we show that TANK-binding kinase 1 (TBK1) serves as a vital regulator of proinflammatory macrophage function and protects against tissue inflammation. Myeloid cell–conditional Tbk1 knockout (MKO) mice spontaneously developed adipose hypertrophy and metabolic disorders at old ages, associated with increased adipose tissue M1 macrophage infiltration and proinflammatory cytokine expression. When fed with a high-fat diet, the *Tbk1*-MKO mice also displayed exacerbated hepatic inflammation and insulin resistance, developing symptoms of nonalcoholic steatohepatitis. Furthermore, myeloid cell–specific TBK1 ablation exacerbates inflammation in experimental colitis. Mechanistically, TBK1 functions in macrophages to suppress the NF-κB and MAP kinase signaling pathways and thus attenuate induction of proinflammatory cytokines, particularly IL-1β. Ablation of IL-1 receptor 1 (IL-1R1) eliminates the inflammatory symptoms of *Tbk1*-MKO mice. These results establish TBK1 as a pivotal anti-inflammatory mediator that restricts inflammation in different disease models.

inflammation | metabolic disorders | fatty liver disease | TBK1 | macrophages

Inflammation is a protective response of the body against harmful stimuli, including microbes, abnormal cells, wounds, and nutritional and environmental factors. Under normal situations, inflammation promotes pathogen clearance and tissue repair and is resolved when dangerous signals are eliminated. However, unresolved inflammatory responses can lead to chronic inflammatory diseases (1), such as inflammatory bowel disease (IBD) (2), obesity (3–5), cardiovascular diseases (6), and cancer (7). Obesity is associated with various metabolic diseases, including nonalcoholic fatty liver disease (NAFLD). Some NAFLD patients develop nonalcoholic steatohepatitis (NASH), an advanced form of NAFLD marked by hepatic inflammation and increased risk for developing insulin resistance, cirrhosis, and liver failure (8, 9). The prevalence and mortality of NASH and other inflammatory diseases have been increasing rapidly in recent years (10, 11), making it vital to understand the molecular mechanisms underlying chronic inflammation.

Macrophages, as a critical component of innate immunity, play an irreplaceable role in inflammatory responses. Tissue infiltration of macrophages is associated with various inflammatory diseases, including obesity (12), atherosclerosis (13), and IBD (14). Depending on their polarization states, macrophages may play pro- or anti-inflammatory functions (15). Classically activated macrophages, known as the M1 type, produce various proinflammatory cytokines such as IL-6, TNF-α, and IL-1 and promote inflammatory responses (15). On the other hand, alternatively activated or M2-type macrophages secrete anti-inflammatory cytokines such as IL-10 and TGFβ (16) and are crucial for resolving inflammation and mediating tissue repair (17, 18). Under normal conditions, the balance between M1 and M2 macrophages is tightly regulated and the population of M1 macrophages temporarily increased during an inflammatory response. Uncontrolled M1 macrophage generation and activation contribute to inflammatory diseases and metabolic disorders.

Macrophages sense infections and other inflammatory triggers via pattern-recognition receptors (PRRs), particularly toll-like receptors (TLRs) (19). Upon stimulation by microbial components or ligands derived from damaged tissues, TLRs transduce signals leading to activation of signaling cascades, including activation of MAP kinases (MAPKs) and IκB kinase (IKK), which activate the transcription factors AP1 and NF-κB, respectively, and

Significance

Macrophages play a crucial role in chronic inflammatory diseases, such as nonalcoholic steatohepatitis (NASH) and inflammatory bowel disease, but how the proinflammatory function of macrophages is controlled is not well understood. In this work, we identified TBK1 as a pivotal anti-inflammatory factor in macrophages that restricts inflammation in different disease models. Myeloid cell–specific TBK1 deficiency causes spontaneous development of metabolic disorders in aged mice and exacerbates high-fat diet–induced fatty liver disease with NASH-like symptoms. The *Tbk1*-MKO mice are also hypersensitive to experimental colitis. We obtained genetic evidence that TBK1 is crucial for controlling proinflammatory signaling pathway in macrophages. These findings establish TBK1 as a pivotal anti-inflammatory factor and a potential therapeutic target for the treatment of inflammatory diseases.

Author contributions: T.G., T.L., C.-J.K., D.J., and L. Zhang designed research; T.G., T.L., C.-J.K., L. Zhang, D.J., X.X., L. Zhu, Y.L., and X.C. performed research; T.G., T.L., and C.-J.K. analyzed data; and T.G., C.-J.K., and S.-C.S. wrote the paper.

Competing interest statement: D.J. is presently an employee of Ziopharm Oncology, Inc., and X.X. is presently an employee of AbbVie, although they participated in this research when they were employed in the University of Texas MD Anderson Cancer Center.

This article is a PNAS Direct Submission.

[1]Present address: Sun Yat-sen University Cancer Center, State Key Laboratory of Oncology in South China, Collaborative Innovation Center for Cancer Medicine, Guangzhou, China 510060.

[2]T.G., T.L., and C.-J.K. contributed equally to this work.

[3]Present address: Department of Laboratory Medicine, West China Second University Hospital, State Key Laboratory of Biotherapy and Collaborative Innovation Center for Biotherapy, Sichuan University, Chengdu, China 610041.

[4]To whom correspondence may be addressed. Email: rex1204@gmail.com or ssun@mdanderson.org.

[5]Present address: Center for Reproductive Medicine, Henan Key Laboratory of Reproduction and Genetics, The First Affiliated Hospital of Zhengzhou University, Zhengzhou, China 450052.

[6]Present address: Research and Development, Ziopharm Oncology, Inc., Boston, MA 02129.

[7]Present address: Pharmacology Division, AbbVie, South San Francisco, CA 94080.

This article contains supporting information online at http://www.pnas.org/lookup/suppl/doi:10.1073/pnas.2107742119/-/DCSupplemental.

Published January 24, 2022.

contribute to the induction of proinflammatory cytokines (20, 21). The macrophage-derived proinflammatory cytokines are major mediators of acute and chronic inflammatory conditions (22, 23). In particular, IL-1β contributes to various inflammatory diseases, including IBD (24), obesity (5, 25), and metabolism disorder (25, 26), and IL-1 blockade has been used as a therapeutic approach to treat patients with a broad spectrum of inflammatory diseases (27). However, despite these extensive studies, how the inflammatory signals are negatively regulated is not well understood.

Tank binding kinase 1 (TBK1) is a member of IKK family and mainly known to mediate type I interferon (IFN) expression in response to viral infections and specific PRR signals (28). However, recent studies suggest that TBK1 responds to a broader range of stimuli (29) and contributes to immune functions other than IFN production (29–32). In the present study, we identified a crucial and unexpected role for TBK1 in restricting inflammatory responses. Myeloid cell–conditional TBK1 knockout (*Tbk1*-MKO) mice spontaneously developed adipose hypertrophy with increased proinflammatory cytokine production at old ages. The myeloid cell–specific TBK1 deletion also sensitizes mice for high-fat diet (HFD)–induced liver inflammation and experimental colitis. We show that TBK1 negatively regulates TLR-stimulated signaling events and production of proinflammatory cytokines, particularly IL-1β.

Results

Aged *Tbk1*-MKO Mice Spontaneously Develop Adipose Hypertrophy with Elevated Proinflammatory Cytokine Expression. To study the role of TBK1 in innate immune cells, we generated *Tbk1*-MKO mice by crossing TBK1-flox mice with Lyz2 Cre mice. These mutant mice and their age-matched wild-type control mice did not show obvious differences in body weight when monitored up to 8 mo of age (Fig. 1*A*). However, 8-mo–old *Tbk1*-MKO mice exhibited significantly increased size and weight of epididymal white adipose tissue (eWAT) (Fig. 1*B*), although this spontaneously developed phenotype was not seen in young adult mice (*SI Appendix*, Fig. S1). Histology analysis revealed adipocyte hypertrophy in the eWAT of *Tbk1*-MKO mice (Fig. 1*C*). Thus, TBK1 deficiency in innate immune (myeloid) cells causes spontaneous development of adipocyte hypertrophy in aged mice.

Macrophages play a crucial role in regulating adipose tissue remodeling, and imbalanced increase of M1 type of proinflammatory macrophages is known to promote adipocyte hypertrophy (33). We thus analyzed the macrophages in eWAT by flow cytometry. The frequency of $CD11b^+F4/80^+$ macrophages was comparable in the wild-type and *Tbk1*-MKO eWAT, but the absolute number of macrophages was significantly increased in the *Tbk1*-MKO eWAT because of its larger mass (Fig. 1*D*). Importantly, the macrophages derived from *Tbk1*-MKO eWAT had a significantly increased frequency of M1 macrophages and decreased frequency of M2 macrophages compared to macrophages derived from wild-type eWAT (Fig. 1*E*). Consistently, the *Tbk1*-MKO eWAT displayed an elevated expression level of messenger RNAs (mRNAs) for the proinflammatory cytokines IL-1β and TNF-α (Fig. 1*F*). The *Tbk1*-MKO eWAT showed an elevated protein level of IL-1β. The TBK1 deficiency also moderately increased the protein level of TNF-α, but this result did not reach statistical significance (Fig. 1*G*). Flow cytometry further demonstrated the increased expression of pro–IL-1β protein in the $CD11b^+F4/80^+$ macrophages of *Tbk1*-MKO eWAT (Fig. 1*H*).

The *Tbk1*-MKO and wild-type control mice did not show a significant difference in liver mass or the percentage of $CD11b^+F4/80^+$ liver tissue macrophages (*SI Appendix*, Fig. S2 *A* and *B*). However, the macrophages derived from the *Tbk1*-MKO mouse liver contained a larger population of M1 macrophages than those from the wild-type mouse liver (*SI Appendix*, Fig. S2*C*), Consistently, qRT-PCR of liver tissue showed a higher level of mRNA expression for the proinflammatory cytokines IL-1β and TNF-α (*SI Appendix*, Fig. S2*D*), but the protein levels of the proinflammatory cytokines were very similar in liver tissues between wild-type and *Tbk1*-MKO mice (*SI Appendix*, Fig. S2*E*), suggesting a different translational control in liver tissues. Together, these results suggest that myeloid cell–specific TBK1 deficiency increases the frequency of M1 macrophages and the production of proinflammatory cytokines in aged mice, which is associated with adipocyte hypertrophy.

HFD-Fed *Tbk1*-MKO Mice Develop NASH-Like Fatty Liver Disease. Our finding that aged *Tbk1*-MKO mice developed hypertrophy accompanied with cytokine overexpression in the eWAT suggested a role for TBK1 in regulating macrophage functions in metabolic inflammation. To further examine this possibility, we employed an HFD-induced metabolic disease model. We fed age-matched *Tbk1*-MKO and wild-type male mice with an HFD or a normal diet beginning at 4 wk of age and monitored body weight and food intake. The *Tbk1*-MKO and wild-type control mice exhibited comparable bodyweight and food intake over the course of HFD treatments (Fig. 2 *A* and *B*). The HFD-treated *Tbk1*-MKO and wild-type control mice also did not show significant differences in eWAT mass or macrophage infiltration (*SI Appendix*, Fig. S3 *A* and *B*). However, the eWAT macrophages of the *Tbk1*-MKO mice contained a markedly higher percentage of M1 and lower percentage of M2 populations (*SI Appendix*, Fig. S3*C*). Consistently, the *Tbk1*-MKO eWAT macrophages displayed a higher level of IL-1β production than the wild-type eWAT macrophages (*SI Appendix*, Fig. S3*D*).

Proinflammatory macrophages critically contribute to the development of metabolic liver disorders, including NASH (34). Interestingly, the HFD-fed *Tbk1*-MKO mice developed severe liver disorders with characteristics of NASH. Both the size and weight of the liver were significantly increased in HFD-fed *Tbk1*-MKO mice compared to the HFD-fed wild-type mice (Fig. 2*C*). The livers of *Tbk1*-MKO mice were also paler than those of the wild-type mice under HFD-fed conditions, indicative of fatty liver (Fig. 2*C*). Indeed, histology analysis revealed enlarged liver cells with abundant fat droplets in the cytoplasm and loss of normal reticular formation in the HFD-fed *Tbk1*-MKO mice, as compared with the HFD-fed wild-type mice (Fig. 2*D*). Liver tissue oil red O staining also showed more accumulation of lipid droplets in the liver of *Tbk1*-MKO mice, confirming the symptom of fatty liver (Fig. 2*E*). Liver disease is often associated with elevated serum concentration of liver enzymes, including alanine aminotransferase (ALT) and aspartate aminotransferase (AST). The *Tbk1*-MKO mice had a significantly higher level of serum AST and ALT than the wild-type mice when fed with HFD (Fig. 2*F*). These results emphasize a role for myeloid TBK1 in regulating metabolic disorders.

To examine the mechanism by which myeloid cell TBK1 regulates HFD-induced liver disease, we analyzed immune cell infiltration. The HFD-fed *Tbk1*-MKO mice displayed much more inflammatory cell clusters in the liver section than the HFD-fed wild-type control mice (Fig. 2*G*). In line with this result, flow cytometry of liver immunocytes detected a significantly increased frequency of $CD11b^+F4/80^+$ macrophages in the HFD-treated *Tbk1*-MKO mice compared to the wild-type mice (Fig. 2*H*). Moreover, the liver macrophages of *Tbk1*-MKO mice consisted of a higher percentage of M1 macrophages and lower percentage of M2 macrophages (Fig. 2*I*). In line with this finding, qRT-PCR analysis showed that the liver tissue of HFD-treated *Tbk1*-MKO mice exhibited an increased level of mRNAs for several proinflammatory

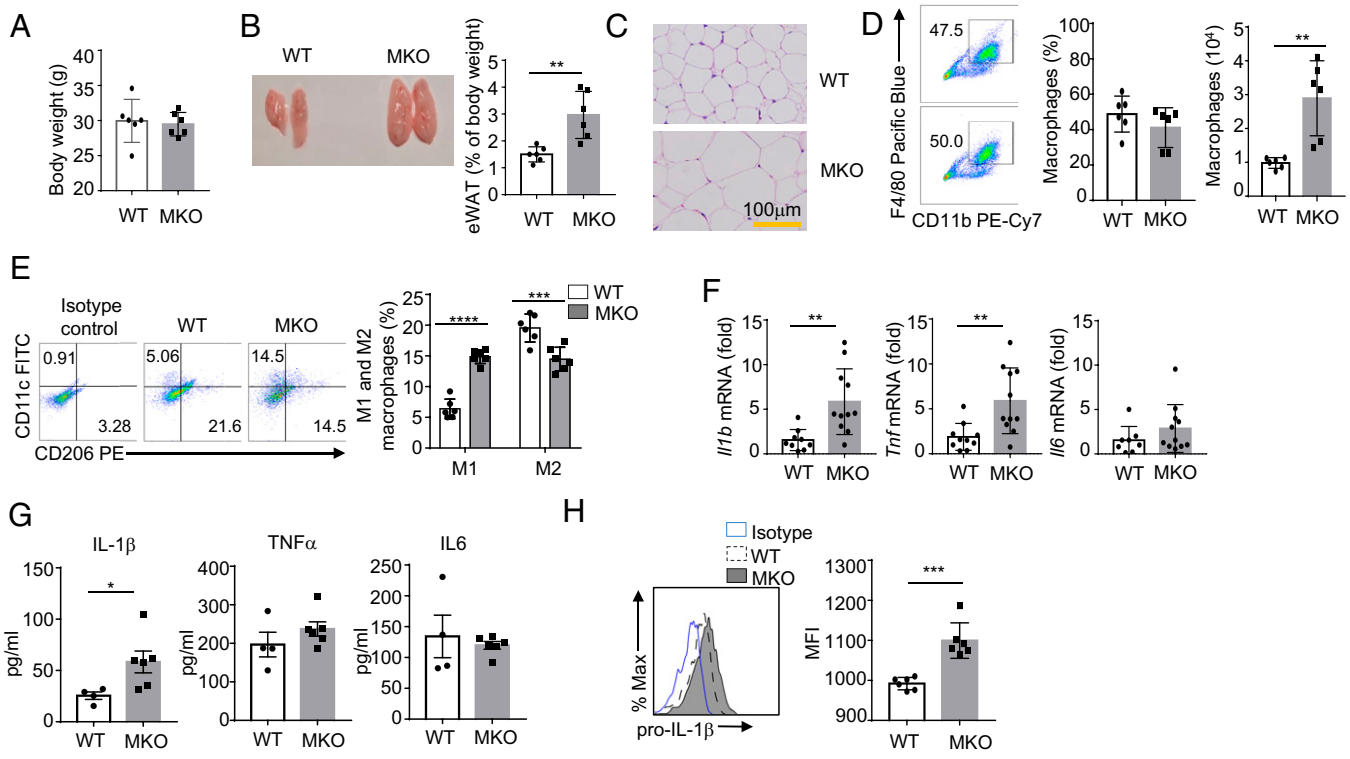

Fig. 1. Aged *Tbk1*-MKO mice display aberrant eWAT expansion, adipocyte hypertrophy, and increased proinflammatory cytokine expression. (*A–C*) Body weight ($n = 6$) (*A*), eWAT picture and weight (presented as percentage of body weight) (*B*), and H&E staining of eWAT sections (*C*) of age-matched (8 mo) *Tbk1*-MKO and wild-type (WT) control male mice. (*D* and *E*) Flow cytometric analysis of the frequency and absolute number of F4/80$^+$CD11b$^+$ macrophages gated on CD45+ cells ($n = 6$) (*D*) and the frequency of M1 (CD206$^-$/CD11c$^+$) and M2 (CD206$^+$/CD11c$^-$) macrophages gated on F4/80$^+$CD11b$^+$ macrophages ($n = 6$) (*E*) in eWAT of WT and *Tbk1*-MKO mice (8 mo old), presented as a representative plot (*Left*) and summary graph based on six pairs of mice (*Right*). (*F*) qRT-PCR analysis of the indicated mRNAs in total eWAT tissue from WT and *Tbk1*-MKO mice ($n = 10$ for WT mice, $n = 11$ for *Tbk1*-MKO mice). (*G*) ELISA analysis of the indicated cytokines in total eWAT tissue from WT and *Tbk1*-MKO mice (WT, $n = 4$; *Tbk1*-MKO, $n = 6$). (*H*) ICS and flow cytometric analysis of intracellular pro–IL-1β in gated eWAT F4/80$^+$CD11b$^+$ macrophages of WT and *Tbk1*-MKO mice (8 mo old). Data are presented as a representative plot (*Left*) and a summary graph of mean fluorescence intensity (MFI) based on six pairs of mice (*Right*). Data are representative of three independent experiments (*A–E* and *H*) or summary of all data from different experiments (*F* and *G*). Summary data are presented as mean ± SD based on multiple mice, with *P* values determined by two-tailed Student's *t* test. $^{**}P < 0.01$; $^{***}P < 0.001$; $^{****}P < 0.0001$.

cytokines, including IL-1β, IL-6, and TNF-α (Fig. 2*J*). Parallel enzyme-linked immunosorbent assay (ELISA) analysis revealed that the protein level of IL-1β was increased in the liver tissue of HFD-treated *Tbk1*-MKO mice compared to wild-type mice (Fig. 2*K*). The TBK1 deficiency also moderately increased the protein level of TNF-α and IL-6, but this result did not reach statistical significance. The increased expression of IL-1β in *Tbk1*-MKO liver macrophages was further confirmed at the protein level by intracellular cytokine staining (ICS) and flow cytometry (Fig. 2*L*). Collectively, these results suggest that myeloid cell–specific TBK1 deficiency sensitizes mice to HFD-induced liver disorder, causing the development of NASH-like symptoms.

Myeloid-Specific TBK1 Deficiency Impairs Glucose Tolerance and Insulin Sensitivity in Aged Mice and HFD-Fed Mice. Low-grade inflammation, mediated by the M1 type of macrophages, induces insulin resistance and glucose intolerance, which in turn contribute to the development of NASH (34). To further elucidate the mechanism by which myeloid TBK1 regulates NASH induction, we examined the potential effect of TBK1 deficiency on glucose metabolism by performing oral glucose tolerance tests (OGTTs) and insulin tolerance tests (ITTs) using aged (12-mo–old) wild-type and *Tbk1*-MKO mice. At the age of 12 mo, *Tbk1*-MKO mice displayed a severe symptom of glucose intolerance, as revealed by the profoundly elevated level of blood glucose and insulin after a glucose load in the OGTT compared to the age-matched wild-type mice (Fig. 3*A*). In ITT, the insulin-induced blood glucose level reduction was significantly attenuated in the *Tbk1*-MKO mice, suggesting impaired insulin sensitivity in these aged mutant mice (Fig. 3*B*). At a younger age (6 mo), the *Tbk1*-MKO mice also showed glucose intolerance, although not insulin resistance (Fig. 3 *C* and *D*). The myeloid cell–specific TBK1 deficiency also promoted glucose intolerance and insulin resistance in HFD-fed young adult mice (Fig. 3 *E* and *F*). Thus, impaired glucose tolerance and insulin sensitivity occur in both aged *Tbk1*-MKO mice and HFD-fed young adult *Tbk1*-MKO mice. These results emphasize a role for myeloid TBK1 in regulating inflammation and metabolic disorders.

TBK1 Suppresses TLR-Induced Proinflammatory Signaling and Cytokine Expression in Macrophages. To further confirm the anti-inflammatory role of TBK1 in macrophages, we examined the effect of TBK1 deficiency on TLR-stimulated proinflammatory cytokine production in bone marrow–derived macrophages (BMDMs). Upon stimulation by the TLR2 ligand Pam3CSK4, the *Tbk1*-MKO BMDMs had profoundly increased induction of mRNAs for IL-1β, IL-6, and TNF-α compared to the wild-type BMDMs (Fig. 4*A*). The TBK1 deficiency also significantly increased the induction of IL-1β, TNF-α, and IL-6 at the protein level (Fig. 4*B*). This result was particularly striking for the induction of IL-1β production. Immunoblot analyses further revealed that the TBK1 deficiency markedly promoted the

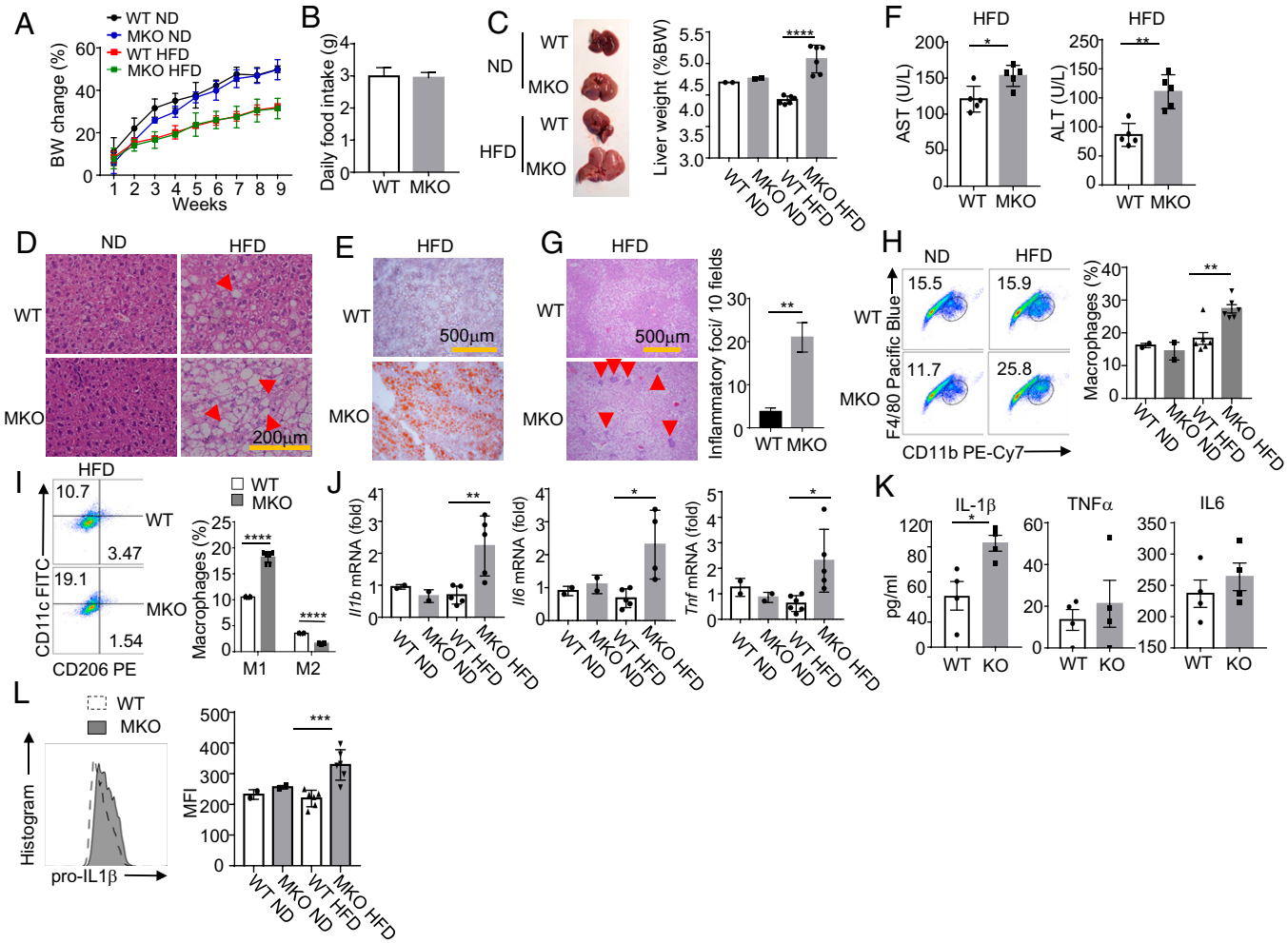

Fig. 2. HFD-fed *Tbk1*-MKO mice develop NASH-like symptoms. Age-matched (4-wk–old) *Tbk1*-MKO and WT control mice were fed with HFD or normal diet (ND) for 9 wk. (*A* and *B*) Body weight (BW) changes (*A*) and average daily food intake (*B*) over the course of 9 wk of HFD or ND feeding ($n = 6$ for HFD-fed mice, $n = 2$ for ND-fed mice). (*C*–*E*) Liver picture and weight (presented as percentage of body weight) (*C*), H&E-stained liver sections with representative lipid droplets indicated by arrowheads (*D*), and oil red O staining of liver sections (*E*) of WT or *Tbk1*-MKO mice after 9 wk of HFD or ND feeding. (*F*) Summary graph of AST and ALT levels in serum of WT or *Tbk1*-MKO mice fed with HFD or ND for 9 wk ($n = 5$). (*G*–*I*) H&E-stained liver sections showing immune cell infiltration by arrowheads (*G*) and flow cytometric analysis of F4/80$^+$CD11b$^+$ liver macrophages gated on CD45$^+$ cells (*H*) or CD206$^-$/CD11c$^+$ (M1) and CD206$^+$/CD11c$^-$ (M2) populations gated on F4/80$^+$/CD11b$^+$ macrophages (*I*). Data are presented as a representative plot (*Left*) or summary graph ($n = 6$ for HFD-fed mice, $n = 2$ for ND-fed mice). (*J*) qRT-PCR analysis of the indicated mRNAs in total liver tissue from WT and *Tbk1*-MKO mice ($n = 5$ for HFD-fed mice, $n = 2$ for ND-fed mice). (*K*) ELISA analysis of IL-1β, TNF-α, and IL-6 levels in the liver tissue of HFD-treated *Tbk1*-MKO mice and WT mice (WT, $n = 4$; MKO, $n = 4$). (*L*) Flow cytometric analysis of intracellular pro-IL1β, gated on F4/80$^+$/CD11b$^+$ liver macrophages. Data are presented as a representative plot (*Left*) and a summary graph of MFI ($n = 6$ for HFD-fed mice; $n = 2$ for ND-fed mice). Data are representative of three independent experiments. Summary data are presented as mean ± SD based on multiple mice, with *P* values determined by two-tailed Student's *t* test. $^*P < 0.05$; $^{**}P < 0.01$; $^{***}P < 0.001$; $^{****}P < 0.0001$.

induction of pro-IL1β expression in response to different TLR ligands (Fig. 4*C*). To ensure that the phenotype was specific to the *Tbk1* deficiency other than a developmental effect, we repeated the experiment using an inducible TBK1 KO model, in which TBK1 was inducibly deleted in BMDMs. We crossed *Tbk1*-flox mice with CreER mice to generate *Tbk1*$^{fl/fl}$CreER and control *Tbk1*$^{+/+}$CreER mice. Isolated BMDMs were then treated with 4-hydroxytamoxifen (4-OHT) for creating TBK1-KO and wild-type control BMDMs. Compared to the wild-type control BMDMs, TBK1 deficiency profoundly increased the production of IL-1β (*SI Appendix*, Fig. S4). This phenotype was consistent with the results from the TBK1 MKO model and further supported the specific role of TBK1 in regulating inflammatory cytokine production. Since LysM-Cre also contribute to loss of TBK1 in neutrophils (35), we further tested the effect of TBK1 on the regulation of inflammatory cytokines in CD11b$^+$Ly6G$^+$ neutrophils. Upon stimulation by Pam3CSK4, the *Tbk1*-deficient peritoneal neutrophils expressed higher levels of IL-1β, IL-6, and TNF-α than wild-type peritoneal neutrophils (*SI Appendix*, Fig. S5), suggesting that neutrophils also played a role in TBK1-mediated inflammatory disorders. Pharmacological inhibition of TBK1 in a human macrophage cell line, THP1, also promoted pro–IL-1β induction by different TLR ligands and the STING ligand cGAMP (*SI Appendix*, Fig. S6). These results suggest that TBK1 negatively regulates proinflammatory cytokine induction by PRR ligands in macrophages and neutrophils.

To determine the mechanism by which TBK1 regulates proinflammatory cytokine induction in macrophages, we examined the role of TBK1 in regulating TLR-stimulated signaling pathways. The TBK1 deficiency substantially enhanced the phosphorylation of p38, ERK, and JNK, MAPK members with crucial roles in the induction of proinflammatory cytokines (Fig. 4*D*). Another important signaling pathway involved in proinflammatory cytokine induction is the IKK/NF-κB pathway. While the TBK1 KO BMDMs displayed drastically higher

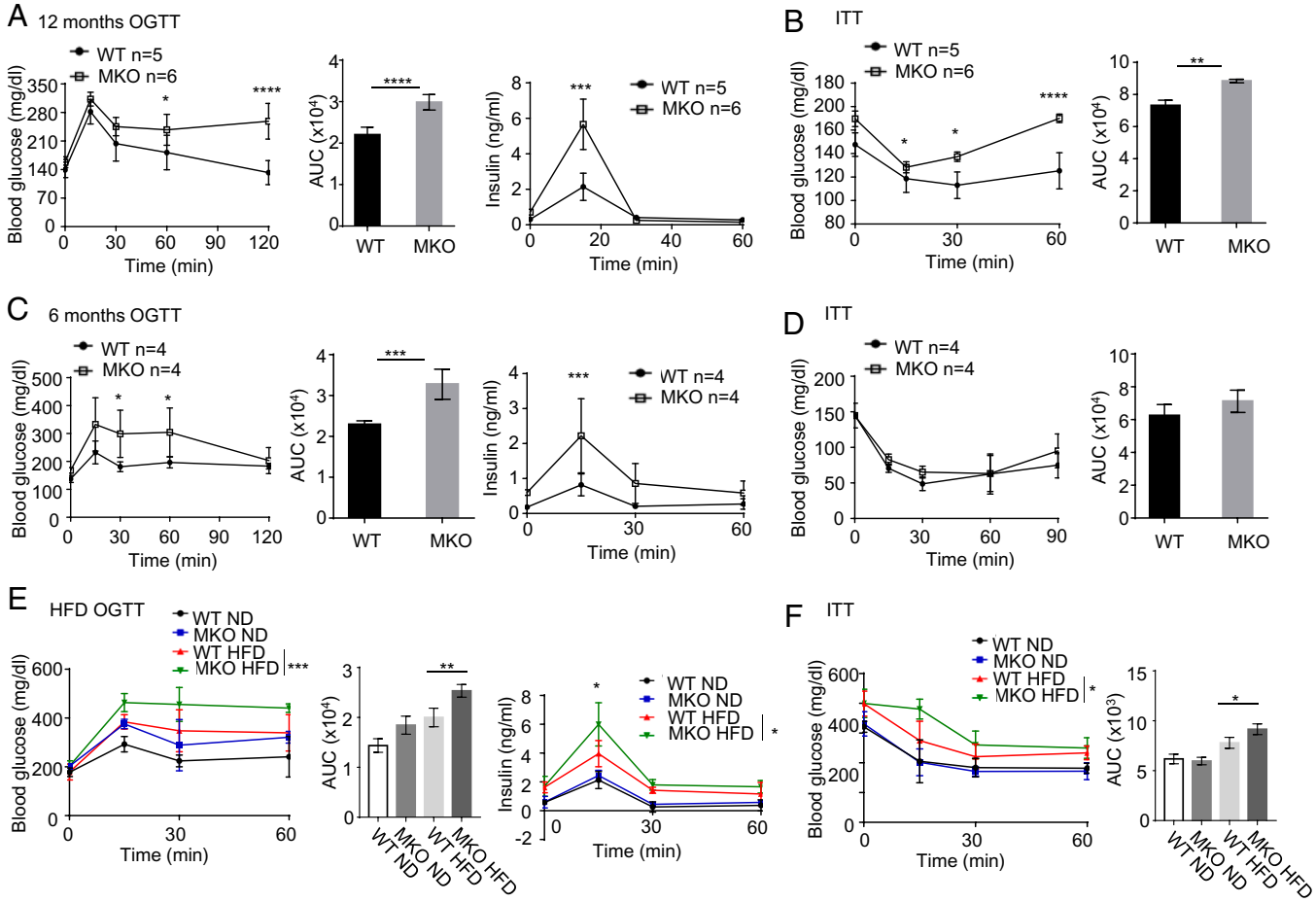

Fig. 3. OGTT and ITT in old mice and HFD-fed mice. (*A–D*) Blood glucose and insulin levels in OGTT (*A* and *C*) and blood glucose levels in ITT (*B* and *D*) as well as summary of area under the curve (AUC) of 12-mo–old ($n = 4$ for WT mice, $n = 6$ for *Tbk1*-MKO mice) (*A* and *B*) or 6-mo–old ($n = 4$) (*C* and *D*) male *Tbk1*-MKO or WT control mice. (*E* and *F*) Results of OGTT and ITT of young adult WT or *Tbk1*-MKO mice fed with HFD or ND for 9 wk ($n = 5$ for HFD-fed mice, $n = 2$ for ND-fed mice). Data are representative of three independent experiments. Summary data are presented as mean ± SEM based on multiple mice, with *P* values determined by two-way ANOVA with Tukey's multiple comparisons test for blood glucose and insulin curves and two-tailed Student's *t* test for the AUC summary curves. $*P < 0.05$; $***P < 0.001$; $****P < 0.0001$.

phosphorylation levels of MEK, ERK, and p38 than wild-type control BMDMs, treatment with an IKK inhibitor, PS1145, largely blocked the induction of MEK/ERK and IL-1β in TBK1 KO BMDMs and erased the differences between the TBK1 KO and wild-type control BMDMs, as well as partially contributing to the regulation of p38 (Fig. 4*E*). The TBK1 deficiency enhanced Pam3CSK4-stimulated phosphorylation of IKK and two major IKK target proteins, the NF-κB inhibitors IκBα and p105 (Fig. 4*F*). Consistently, the Pam3CSK4-induced nuclear expression of the prototypical NF-κB subunits p65 and p50 was also increased in TBK1-deficient macrophages (Fig. 4*F*). To examine the functional significance of these signaling changes, we examined the effect of MAPK and NF-κB inhibitors on IL-1β induction. We employed two different p38 inhibitors, BIRB796 and SB203580; SB203580 inhibits the catalytic activity of p38, whereas BIRB796 inhibits both the phosphorylation and catalytic activity of p38 (36). Importantly, both of these two selective inhibitors of p38 potently inhibited the induction of pro–IL-1β (Fig. 4*G*). Incubation of the cells with an NF-κB–selective inhibitor, JSH-23, also inhibited the induction of pro–IL-1β (Fig. 4*H*). In order to explore the mechanism, we tested the kinase activity of transforming growth factor-β activated kinase 1 (TAK1) and tumor progression locus 2 (TPL2), the regulators for MEK/ERK, JNK, and p38, in wild-type and TBK1 KO BMDMs; the result shows that the kinase activity of TAK1 was comparable between wild-type and TBK1 BMDMs upon the treatment of Pam3CSK4 (*SI Appendix*, Fig. S7). Interestingly, the kinase activity of TPL2 was increased in the TBK1 KO BMDMs upon the treatment of Pam3CSK4 compared to wild-type BMDMs, suggesting that TPL2 may participate in the regulation of MEK/ERK and p38 by TBK1 (Fig. 4*I*). Glycolysis is critical for the regulation of inflammatory response, and the activation of TLR signaling increases glycolysis (37–39). We performed Seahorse extracellular flux analyses to measure extracellular acidification rate (ECAR), which is an indicator of aerobic glycolysis. Treatment of Pam3CSK4 led to induction of glycolysis; however, the glycolysis was comparable between wild-type and TBK1 KO BMDMs (*SI Appendix*, Fig. S8). Together, these results suggest that TBK1 controls TLR-stimulated activation of MAPK and NF-κB signaling pathways and thereby the induction of proinflammatory cytokines.

IL-1R Ablation Prevents the Adipose Tissue and Liver Abnormalities of *Tbk1*-MKO Mice. As described above, TBK1 deficiency promotes induction of proinflammatory cytokines, most strikingly IL-1β. To address the functional significance of TBK1-mediated regulation of IL-1β induction, we crossed *Il1r1*-KO mice with *Tbk1*-MKO mice to generate mice harboring IL-1R1 deficiency and myeloid cell–conditional TBK1 deletion, hereafter called double KO (dKO) mice. Remarkably, while the old *Tbk1*-MKO

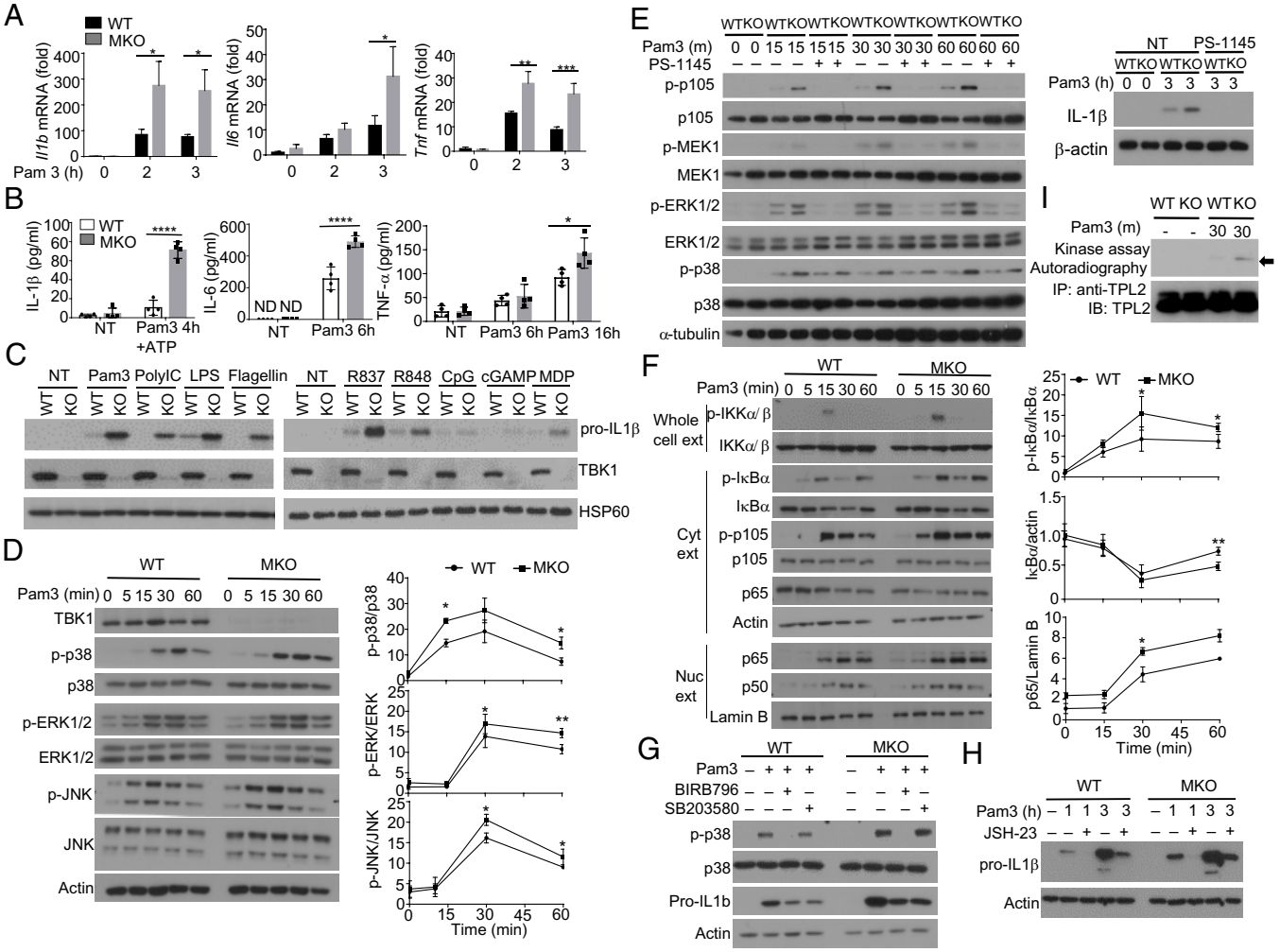

Fig. 4. TBK1 negatively regulates TLR-stimulated signaling and proinflammatory cytokine expression. (*A* and *B*) qRT-PCR (*A*) and ELISA (*B*) analysis of the indicated cytokines in BMDMs derived from WT or *Tbk1*-MKO mice, stimulated with Pam3CSK4 as indicated. NT, nontreated. (*C*) Immunoblot analysis of pro–IL-1β in whole-cell lysates of WT or *Tbk1*-MKO (KO) BMDMs stimulated for 6 h by the indicated TLR ligands or the STING ligand cGAMP and the NOD2 ligand muramyl dipeptide (MDP). (*D*) Immunoblot analysis of the indicated phosphorylated (p-) and total proteins in whole-cell extracts. Data are presented as a representative blot (*Left*) and summary graphs of densitometric quantifications of the indicated proteins (presented as phosphorylated/total protein ratio) based on three independent experiments. The values were normalized to time point 0 of WT cells. (*E*) Immunoblot analysis of the indicated phosphorylated (p-) and total proteins in whole-cell extracts. BMDMs were activated for indicated time with Pam3CSK4 in the presence of solvent control (DMSO) or PS-1145 (10 μM). (*F*) Immunoblot analysis of the indicated phosphorylated (p-) and total proteins in whole-cell extracts (*Top*) and cytoplasmic and nuclear extracts (*Middle* and *Bottom*) of Pam3CSK4-stimulated WT or *Tbk1*-MKO BMDMs. Data are presented as a representative blot (*Left*) and summary graphs of densitometric quantifications of the indicated proteins based on three independent experiments. The values were normalized to time point 0 of WT cells. (*G* and *H*) Immunoblot analysis of the indicated phosphorylated (p-) or total proteins in whole-cell extracts of WT or *Tbk1*-MKO BMDMs stimulated with Pam3CSK4 in the presence (+) or absence (–) of the indicated MAPK inhibitors, BIRB796 (500 nM) and SB203580 (10 μM) (*G*), or the NF-κB inhibitor JSH-23 (50 μM) (*H*). (*I*) BMDMs were stimulated with Pam3CSK4 for the indicated times and subjected to IP using anti-Tpl2 Ab, followed by kinase assays using GST-MEK1 as substrate (*Upper*). Immunoblot analysis of TPL2 (*Lower*). Black arrow indicates the signal of ^{32}p-GST-MEK1.

mice displayed aberrantly increased eWAT mass and adipocyte hypertrophy, the age-matched dKO mice did not show this phenotype, suggesting the critical involvement of IL-1R signaling in this disorder (Fig. 5 *A* and *B*). IL-1R ablation also prevented the aberrant increase of M1 type macrophages in the eWAT of aged *Tbk1*-MKO mice (Fig. 5*C*). These results suggest that hyperproduction of IL-1β in TBK1-deficient macrophages may contributes to the low-grade inflammation and adipocyte hypertrophy of old *Tbk1*-MKO mice.

We then analyzed the effect of IL-1R deletion on the metabolic disorders of HFD-fed *Tbk1*-MKO mice. As expected, under HFD-feeding conditions, the young adult *Tbk1*-MKO mice displayed liver enlargement and dysfunction, as revealed by increased concentrations of the liver enzymes AST and ALT in the serum (Fig. 5 *D* and *E*). However, these metabolic abnormalities were not detected in the IL-1R–deficient *Tbk1*-MKO (dKO) mice (Fig. 5 *D and E*). The massive lipid droplet accumulation and inflammatory cell infiltration in the liver tissue of HFD-fed *Tbk1*-MKO mice were also largely prevented by *Il1r1* deletion (Fig. 5 *F* and *G*). Furthermore, the dKO mice did not display the increased frequencies of total and M1-type liver macrophages observed in the *Tbk1*-MKO mice (Fig. 5 *H* and *I*). Finally, *Il1r1* deletion in *Tbk1*-MKO mice also prevented their development of glucose intolerance induced by HFD (Fig. 5*J*). Together, these results suggest that IL-1 signaling critically contributes to the metabolic disorders of *Tbk1*-MKO mice developed both spontaneously in old ages and inducibly in young ages by HFD feeding.

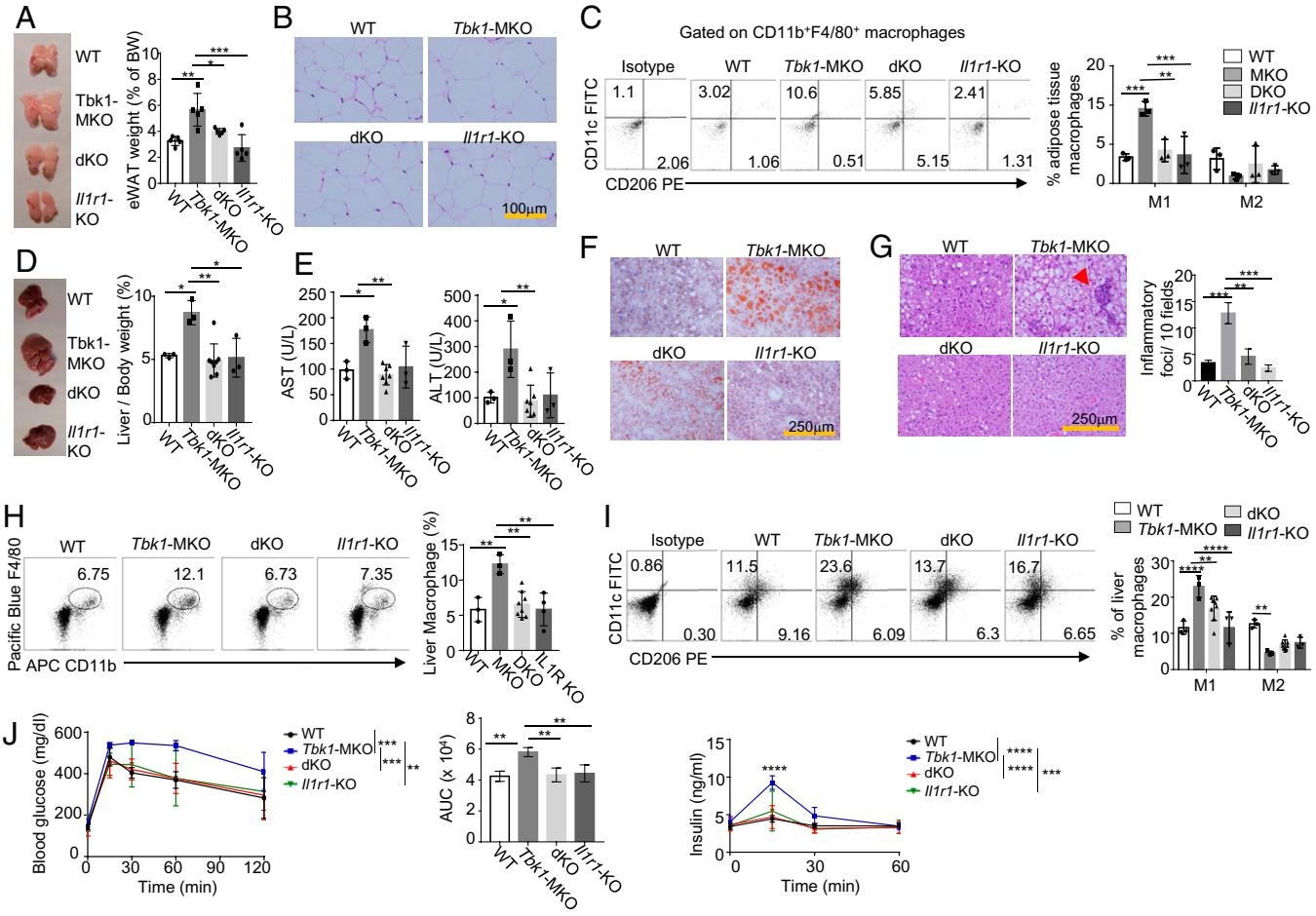

Fig. 5. Deletion of IL-1R attenuates the metabolic disorders of *Tbk1*-MKO mice. (*A–C*) Representative pictures and weight (presented as percentage of body weight) of eWAT (n = 5) (*A*), H&E-stained eWAT sections (*B*), and flow cytometric analysis of $CD206^{-}CD11c^{+}$ (M1) and $CD206^{+}CD11c^{-}$ (M2) populations of gated $F4/80^{+}/CD11b^{+}$ eWAT macrophages (*C*) of 12-mo–old WT, *Tbk1*-MKO, *Tbk1*-MKO/*Il1r1* dKO, and Il1r1-KO mice (n = 3). (*D–I*) Representative pictures and mass (presented as percentage of body weight) of the liver (n = 3 for WT and *Tbk1*-MKO mice, n = 7 for dKO mice, and n = 3 for Il1r1-KO mice) (*D*), serum AST and ALT levels (*E*), oil red O staining of liver sections (*F*), and H&E-stained liver sections (*G*) and flow cytometric analysis of $F4/80^{+}CD11b^{+}$ liver macrophages gated on CD45+ cells (*H*) or $CD206^{-}CD11c^{+}$ (M1) and $CD206^{+}CD11c^{-}$ (M2) populations within the gated $F4/80^{+}/CD11b^{+}$ macrophages (*I*) of the indicated mouse genotypes fed with HFD for 12 wk. (*J*) Blood glucose and insulin levels and AUC in OGTT of the indicated genotypes of mice fed with HFD for 12 wk (n = 4 for WT mice, n = 3 for *Tbk1*-MKO mice, n = 5 for dKO mice, and n = 3 for Il1r1-KO mice). Data are representative of three independent experiments. Summary data are presented as mean ± SD based on multiple mice, with P values determined by two-way ANOVA with Tukey's multiple comparisons test (*J*, blood glucose and insulin curves) and two-tailed Student's t test (*A*, *C–E*, *G–I*, AUC graph of *J*). *P < 0.05; **P < 0.01; ***P < 0.001; ****P < 0.0001.

Myeloid Cell TBK1 Suppresses Experimental Colitis. To investigate whether myeloid cell TBK1 also regulates other types of inflammatory diseases, we employed a widely used experimental colitis model, involving feeding mice with drinking water supplemented with dextran sulfate sodium (DSS), known to damage the epithelial barrier, leading to commensal bacterial invasion and inflammation (40). Interestingly, DSS treatment caused a substantial increase in the level of phosphorylated TBK1 in colonic macrophages, but not in splenic macrophages, suggesting TBK1 activation in intestinal macrophages along with DSS-induced colitis (Fig. 6*A*). To determine the role of myeloid cell TBK1 in regulating colon inflammation, we treated the wild-type or *Tbk1*-MKO mice with 3% DSS in drinking water. Of the wild-type mice, 80% survived the treatment up to 20 d, but only 20% of *Tbk1*-MKO mice survived under the same conditions (Fig. 6*B*). The *Tbk1*-MKO mice also experienced more severe body weight loss and colon shortening, characteristic of colitis (Fig. 6 *C* and *D*). Consistently, the *Tbk1*-MKO mice displayed higher disease activity index scores than wild-type mice on days 6 and 8 of DSS treatment (Fig. 6*E*). Histology analysis revealed substantially more severe inflammation and tissue damages in the distal colon of *Tbk1*-MKO mice compared with that of wild-type mice (Fig. 6*F*). Quantitative analysis also revealed significantly higher histological colitis scores in the colon of *Tbk1*-MKO mice (Fig. 6*G*). Thus, myeloid cell TBK1 plays a crucial role in preventing colon inflammation in the DSS colitis model.

We next examined the effect of TBK1 deficiency on proinflammatory cytokine induction during DSS-mediated colitis induction. Compared to wild-type mice, the *Tbk1*-MKO mice had significantly increased serum concentration of several proinflammatory cytokines, including IL-1β, TNF-α, IL-6, and IL-12, on day 8 of DSS treatment (Fig. 6*H*). At an early time point (day 4), IL-1β was the predominant cytokine aberrantly produced in the *Tbk1*-MKO mice, indicative of a primary role in colitis induction (Fig. 6*I*). To test this possibility, we injected the mice with a combination of anti–IL-1β and anti–IL-1R blocking antibodies to disrupt IL-1 function. IL-1 neutralization significantly protected the wild-type and *Tbk1*-MKO mice from DSS-induced body weight loss, especially during the late time point (day 8) (Fig. 6*J*). The IL-1 blockade also substantially reduced the disease activity index, erasing the differences between the wild-type and *Tbk1*-MKO mice (Fig. 6*K*).

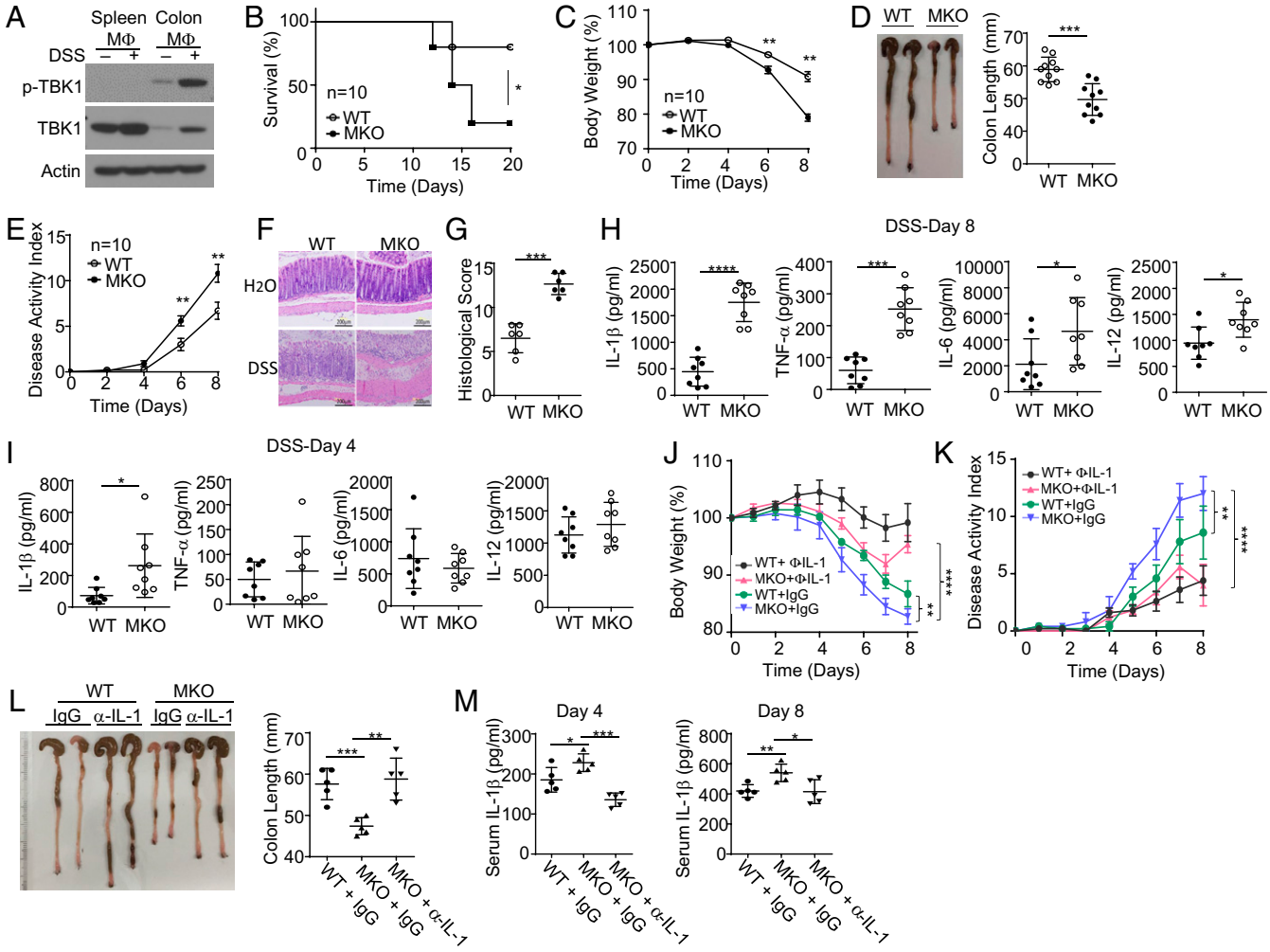

Fig. 6. Myeloid cell TBK1 suppresses DSS-induced colitis. (*A*) Immunoblot analysis of phosphorylated (p-) and total TBK1 in F4/80+ macrophages sorted from the spleen and colon lamina propria of WT mice treated with (+) or without (−) DSS drinking water for 5 d, followed by regular drinking water for 2 d. (*B*) Survival curve of WT and *Tbk1*-MKO mice treated with 3.0% DSS drinking water for 7 d and then fed with regular drinking water for the rest of time. (*C–G*) Body weight changes (*C*), day 8 colon lengths (*D*), DAI (*E*), H&E-stained day 8 colon sections (*F*), and histology scores of day 8 colon sections (*G*) of WT and *Tbk1*-MKO mice treated with 3.5% DSS drinking water for 5 d and then fed with regular drinking water for 3 d. (*H* and *I*) ELISA of serum cytokines on day 8 (*H*) or day 4 (*I*) of WT or *Tbk1*-MKO mice treated with 3.5% DSS drinking water for 5 d and then fed with regular drinking water for 3 d. (*J–M*) Body weight changes (*J*), DAI (*K*), colon lengths on day 8 (*L*), and serum IL-1β concentration on days 4 and 8 (*M*) of WT or *Tbk1*-MKO mice treated with 3.5% DSS drinking water for 5 d and then fed with regular drinking water for 3 d. The mice were also injected i.p. with anti–mIL-1β (200 μg/mouse) plus anti-mIL1R (200 μg/mouse) (marked as anti–IL-1) or Armenian hamster IgG control were used as control on days 0, 2, and 4. Summary data are presented as mean ± SD based on multiple mice, with *P* values determined by Kaplan-Meier analyses with the log-rank Mantel-Cox test (*B*), two-way ANOVA with Tukey's multiple comparisons (*J* and *K*), or two-tailed Student's *t* test (*C–E*, *G–I*, *L*, *M*). $^{*}P < 0.05$; $^{**}P < 0.01$; $^{***}P < 0.001$; $^{****}P < 0.0001$.

Moreover, the colon shortening was also largely rescued in mice treated with anti–IL-1β and anti–IL-1R (Fig. 6*L*). Parallel ELISA revealed that the anti–IL-1β treatment reduced the serum IL-1β concentration of *Tbk1*-MKO mice to a level similar to or lower than that of the wild-type mice (Fig. 6*M*). These results suggest that myeloid cell TBK1 prevents DSS colitis by controlling the production of IL-1β.

Discussion

TBK1 is a major innate immune kinase known to mediate type I IFN induction in response to viral infections. However, the role of TBK1 in regulating inflammatory responses is elusive. In the present study, we obtained genetic evidence that TBK1 serves as a pivotal negative regulator of inflammatory responses. Mice lacking TBK1 in myeloid cells spontaneously developed adipose abnormalities characterized by epididymal fat pad expansion associated with adipocyte hypertrophy. The TBK1 deficiency also exacerbated HFD-induced fatty liver disease associated with inflammation in both the liver and adipose tissue. In addition to these metabolic disorders, the *Tbk1*-MKO mice were hypersensitive to DSS-induced colitis. Consistent with these disease model studies, we found that the TBK1 deficiency in macrophages promotes production of proinflammatory cytokines, particularly IL-1β. Genetic ablation of IL-1R1 largely prevented the inflammatory disorders of the *Tbk1*-MKO mice. These findings establish TBK1 as an anti-inflammatory kinase and a potential target for the treatment of inflammatory diseases.

Adipose tissue, particularly visceral adipose tissue, plays a vital role in the development of metabolic disorders such as insulin resistance, obesity, and metabolic inflammation (41, 42). Aging is associated with visceral fat storage, low-grade inflammation, and increased risk of metabolic diseases (43, 44). The molecular mechanism underlying age-associated adipose tissue

abnormalities and metabolic syndromes is not fully understood. Our present study provides a molecular link of the innate immune system with age-related adipose tissue disorder. At the age of 8 mo or older, the *Tbk1*-MKO mice spontaneously developed abnormal eWAT expansion and adipocyte hypertrophy, associated with impaired glucose tolerance and insulin sensitivity. These aged mutant mice have increased frequency of M1-type macrophages and expression levels of proinflammatory cytokines, especially IL-1β, in eWAT. Importantly, disruption of IL-1–induced signaling by IL-1R1 ablation ameliorates the metabolic disorders of the *Tbk1*-MKO mice. Based on these findings, we propose that TBK1 deficiency causes aberrant proinflammatory cytokine production by adipose tissue macrophages, thereby inducing abnormal eWAT expansion and metabolic disorders. Our data are in line with a previous study suggesting that local proinflammatory responses are crucial for adipose tissue expansion and remodeling under both physiological and HFD-fed conditions (45). It is thus likely that TBK1 in myeloid cells maintains adipose tissue homeostasis through controlling the proinflammatory function of macrophages.

Another remarkable function of TBK1 uncovered in the present study is the regulation of HFD-induced liver disease. When fed with HFD for 9 wk, the *Tbk1*-MKO mice displayed severe fatty liver symptoms, characterized by steatosis, inflammation, and increased AST and ALT serum concentrations indicative of liver damage. These symptoms are typical features of NASH, an inflammatory and advanced form of NAFLD that can further progress to cirrhosis (8, 9). Under the same conditions, the wild-type control mice only had minor symptoms, highlighting a critical role for myeloid cell TBK1 in preventing NASH development. While many factors contribute to the development of NASH, liver innate immune cells (macrophages and neutrophils) act as key metabolic sensors and inflammatory mediators (46, 47). These innate immune cells respond to damage-associated molecular patterns released by damaged hepatocytes via PRRs, particularly TLRs, and produce proinflammatory cytokines. We found that TBK1-deficient macrophages display the M1 phenotype and produce increased levels of proinflammatory cytokines in the liver of HFD-fed mice. It is important to note that the TBK1 deficiency promotes NASH-like disease without affecting the HFD-induced body weight gain. These results suggest that the proinflammatory function of TBK1-deficient macrophages contributes to the development of NASH-like disease in HFD-fed *Tbk1*-MKO mice. This idea is further supported by our finding that IL-1R1 deletion ameliorates the NASH-like disease of *Tbk1*-MKO mice.

Our present study reviewed that TBK1 deficiency enhanced the phosphorylation of IKK as well as the MAPKs ERK, JNK, and p38 in BMDMs. TAK1 functions as an upstream modulator of IKK, MAPK, and p38 signaling (48), and TBK1 deficiency in mouse embryonic fibroblasts promotes the activation of TAK1. However, we found that the Pam3CSK4-stimulated kinase activity of TAK1 was not altered by TBK1 deletion in BMDMs. TPL2 has been reported to mediate IKK signaling for the activation of MEK/ERK and p38 (49–51). Interestingly, the Pam3CSK4-stimulated TPL2 kinase activity was increased in the TBK1 KO BMDMs compared to wild-type BMDMs, suggesting the involvement of TBK1 in regulating TPL2 signaling axis. In this regard, a previous study suggests that TBK1 and IKKe phosphorylate the catalytic subunits of IKK and its regulatory subunit, NEMO, to negatively regulate IKK activity (52). Our finding that IKK is hyperactivated in TBK1-deficient macrophages is consistent with this prior study. Since IKK is an upstream activator of Tpl2, it is possible that TBK1 negatively regulates the proinflammatory TLR signaling through controlling IKK activity. It has also been suggested that TBK1 suppresses inflammation by inducing the phosphorylation and degradation of noncanonical NF-κB–inducing kinase (NIK), thus attenuating NF-κB activity (53). NIK was observed to be up-regulated in liver steatosis and regulate alcoholic steatosis through modulating of PPARα phosphorylation and recruitment of ERK1/2 and MEK1/2 (54). We have previously shown that TBK1 functions as a negative regulator NIK in B cells (30). Whether NIK may play a role in TBK1-mediated NASH needs further investigation. Notwithstanding, our findings suggest that TBK1 may regulate MEK/ERK and p38 signaling through the modulation of TPL2.

Our data suggest that TBK1 in myeloid cells restricts inflammatory responses in different disease models. In addition to metabolic diseases, TBK1 suppresses colitis induced by DSS, which is known to damage the epithelial barrier, leading to commensal bacterial invasion and induction of proinflammatory cytokine expression in lamina propria innate immune cells (40). Consistently, we found that TBK1 suppresses TLR-stimulated proinflammatory cytokine expression in macrophages. Although TBK1 is a well-known mediator of type I IFN expression, the anti-inflammatory function of TBK1 is independent of type I IFNs, since TBK1 deficiency promotes proinflammatory cytokine induction by both TLR ligands that induce type I IFNs (lipopolysaccharide [LPS] and polyinosinic–polycytidylic acid) and TLR ligands that do not induce type I IFN (Pam3CSK4 and flagellin). Our data suggest that TBK1 controls TLR-stimulated activation of MAPK pathways and the IKK/NF-κB pathway, which are known to be required for proinflammatory cytokine gene induction. Collectively, our work establishes TBK1 as a pivotal anti-inflammatory kinase and a potential therapeutic target for treating inflammatory diseases.

Materials and Methods

Mice. *Tbk1*-flox mice were generated in a B6 × 129 mixed genetic background (30) and further backcrossed to B6 background for four generations. These mice were crossed with LysM^{cre} (B6.129P2-Lyz2$^{tm1(cre)Ifo}$/J) mice from Jackson Laboratory to generate *Tbk1*$^{+/+}$LysM^{cre} (wild-type) and *Tbk1*$^{fl/fl}$LysM^{cre} (*Tbk1*-MKO) mice. *Il1r1*-KO (B6.129S7-*Il1r1*^{tm1Imx}/J) mice were obtained from Jackson Laboratory. *Tbk1*-MKO mice were crossed with *Il1r1*-KO mice to generate age-matched wild-type, *Tbk1*-MKO, *Il1r1*-KO, and *Il1r1*-KO/*Tbk1*-MKO (dKO) mice. All mice were on a C57BL/6 genetic background and maintained in a specific-pathogen–free facility of the University of Texas MD Anderson Cancer Center, and all animal experiments were carried out in accordance with protocols approved by the Institutional Animal Care and Use Committee of the University of Texas MD Anderson Cancer Center.

Antibodies. Fluorescence-labeled anti-mouse antibodies CD45 (30-F11, PerCP-Cy5.5), F4/80 (Clone: BM8.1, Pacific Blue), CD11b (ICRF44, phycoerythrin [PE]-Cy7), CD11c (N418, fluorescein isothiocyanate [FITC]), CD206 (MMR, PE), and IL1b (Proform) (NJTEN3, allophycocyanin) were purchased from eBioscience.

Anti-actin (3700, 1:10,000), TBK1 (3504, 1:1,000), phospho-p38 MAPK (9215, 1:1,000), phosphor-ERK (9101, 1:1,000), phosphor-JNK (4668, 1:1,000), JNK (4672, 1:1,000), phospho-IKKα/β (2697, 1:1,000), IKKα (2682, 1:1,000), phosphor-IκBα (9241, 1:1,000), IκBα (4814, 1:1,000), p65(8242, 1:1,000), phospho-NF-κB p105 (Ser932) (18E6) (4806, 1:1,000), NF-κB1 p105/p50 (D4P4D) (13586, 1:1,000), and lamin B (12586, 1:1,000) were from CST. HSP60 (sc-13115, 1:1,000), p38 (7149, 1:1,000), ERK (sc-514302, 1:1,000), ASC (SC-271514, 1:1,000), and Cot (SC-720, 1:1,000) were from Santa Cruz. IL1β (AF-401-SP, 1:1,000) was from R&D. Anti-Caspase-1 (p20) (AG-20B-0042-C100, 1:1,000) was from Adipogen.

HFD Treatment of Mice. Age-matched (4-wk-old) male mice of the indicated genotype were fed with an HFD (60% Energy, Test Diet) or a normal diet control (Lab diet 5030) for the indicated time periods and monitored for body weight changes every 7 d. At the indicated time point, the mice were killed, and eWAT and liver were collected for histology analysis and flow cytometry analysis of tissue immunocytes.

Isolation and analysis of adipose tissue immunocytes. Adipose tissues were excised, minced, and digested with collagenase II (4 mg/mL; Sigma-Aldrich) for 20 min at 37 °C. After digestion, cell suspensions were passed through a 70-μm cell strainer to yield single-cell suspensions. Immunocytes were purified by centrifugation (400 × *g*) at room temperature for 30 min over a 30/70% discontinuous Percoll gradient. The cells were collected from the interphase, thoroughly washed, and analyzed by flow cytometry.

Isolation and analysis of liver immunocytes. Liver tissues were excised, minced, and digested with collagenase IV (0.5 mg/mL; Sigma-Aldrich) and DNase I (0.1 mg/mL; Roche) for 40 min at 37 °C. After digestion, cell suspensions were

passed through a 70-μm cell strainer to yield single-cell suspensions. Immunocytes were purified by centrifugation (400 × *g*) at room temperature for 30 min over a 30/70% discontinuous Percoll gradient. The cells were collected from the interphase, thoroughly washed, and analyzed by flow cytometry.

Histological analysis. Mouse epididymal adipose tissues, liver, or colon tissues were fixed overnight with 4% paraformaldehyde, and the paraffin-embedded sections (8 μm) were then stained with hematoxylin and eosin (H&E). Frozen liver tissue was made in optimal cutting temperature compound and cut into 8- to 10-mm sections. The frozen sections were fixed in formalin and stained with freshly prepared oil red O working solution.

Flow cytometry and ICS. Cells were stained with the indicated fluorescence-conjugated antibodies and subjected to flow cytometry analysis and cell sorting as previously described (55) using FACS Fortessa and FACSAria (BD Biosciences). For ICS, immunocytes isolated from the adipose tissues or liver of the indicated mice were stimulated for 4 h with LPS (100 ng/mL) in the presence of monensin (10 μg/mL) during the last 2 h and then subjected to ICS and flow cytometry analyses. The data were analyzed using FlowJo software.

OGTT and ITT assay. For OGTT, mice were fasted overnight while having access to drinking water and administered with glucose solution (Sigma-Aldrich) via oral gavage (2 g glucose/kg body weight). Blood samples were collected (~30 μL) at the indicated time points of glucose administration and used for measuring glucose levels with a glucometer and insulin levels by Ultrasensitive Mouse Insulin ELISA kit (Crystam Chem). For ITT, mice were fasted for 2 h before insulin injection while ensuring that the mice had access to drinking water. Insulin (Novo Nordisk) was injected intraperitoneally (0.35 to 0.75 U insulin/kg body weight). Blood glucose levels were measured before and after the indicated time points of insulin injection.

ELISA and qRT-PCR. Mouse sera or in vitro cell culture supernatants were analyzed by ELISA using a commercial assay system (eBioScience). Total RNA was extracted with TRIzol reagent from the indicated cells and subjected to qRT-PCR using SYBR reagent (Bio-Rad). Gene-specific primers are listed in *SI Appendix*, Table S1.

Immunoblot assay. For whole-cell extract preparation, sorted tissue macrophages, BMDMs, or THP1 cells were lysed in radioimmunoprecipitation assay buffer containing 50 mM Tris·HCl (pH 7.4), 150 mM NaCl, 1% Nonidet P-40, 0.5% sodium deoxycholate, 1 mM ethylenediaminetetraacetic acid (EDTA), 1 mM dithiothreitol, 1 mM sodium orthovanadate, 5 mM sodium fluoride, 20 mM p-nitrophenyl phosphate, 1 mM phenylmethylsulfonyl fluoride, 1 mg/mL pepstatin, and 1 mg/mL aprotinin. Cytoplasmic and nuclear extracts were prepared as previously described (56). The cell extracts were subjected to immunoblot assays as described (57).

DSS-induced colitis. For lethality analysis, age- and sex-matched littermate wild-type and TBK1 KO mice were used to minimize individual variations. The mice were supplied with 3.0% DSS in drinking water (MP Biomedicals) for 7 d, which was then replaced with normal drinking water for the rest of the experimental time. The treated mice were monitored every other day, and moribund mice were killed based on protocols approved by the Institutional Animal Care and Use Committee of the University of Texas MD Anderson Cancer Center. For inflammation studies, mice were treated with 3.5% DSS in drinking water for 5 d and then supplied with regular drinking water for 3 d. Body weight was measured every other day for up to 8 d, and the mice were then killed for measuring colon length, histology analysis, and blood collection for ELISA.

For neutralization antibody treatment, colitis was induced by the oral administration of 3.5% DSS for 5 d. Anti–mIL-1β (200 μg/mouse) and anti–mIL-1R (200 μg/mouse) were intraperitoneally administered on days 0, 2, and 4. Armenian hamster IgG were used as control. Time courses of body weight change and disease activity index (DAI) were monitored daily. DAI was scored basted on the criteria summarized in *SI Appendix*, Table S2 and presented as a total score (general appearance + body weight loss + feces consistency + rectal bleeding).

Histological analysis was performed on colorectum near the anus and scored based on the criteria summarized in *SI Appendix*, Table S3. The final scores are the sum of the four parts, including the inflammation severity, depth of injury, crypt damage, and percentage of area involved.

In vitro experiments with thioglycolate-elicited neutrophils. The mice were injected with 1.5 mL of 4% thioglycolate broth (BD, 211716) into the peritoneal cavity of the mouse. After 3 h incubation, the mice were killed to prepare a single-cell suspension of elicited peritoneal cells. Elicited peritoneal neutrophils were further isolated using anti-Ly6G beads. The isolated neutrophils were stimulated for 3 h with Pam3CSK4and then subjected to qRT-PCR analysis.

In vitro kinase assays. BMDMs were stimulated for the indicated time with Pam3CSK4. The cells were then harvested with cell lysis buffer [1% Nonidet P-40, 20 mM Hepes (pH 7.6), 250 mM NaCl, 20 mM β-glycerophosphate, 1 mM EDTA, 1 mM dithiothreitol (DTT), 20 mM p-nitrophenyl phosphate, 1 mM phenylmethylsulfonyl fluoride, 1 mg/mL pepstatin, and 1 mg/mL aprotinin] and then subjected to immunoprecipitation and kinase assay. The antibodies against TPL2 or TAK1 were incubated for 45 min with the cell lysates. After 45 min, the protein A/G agarose was added into the tubes and continued to incubate for 2 more hours. The samples were washed with lysis buffer three times and kinase assay buffer [20 mM Hepes (pH 7.6), 20 mM $MgCl_2$, 20 mM β-glycerophosphate, and 1 mM EDTA] containing 1 mM DTT twice. The immunoprecipitation (IP) samples were then incubated for 30 min at 30 °C with kinase assay buffer containing 20 μM ATP, 2 mM DTT, 0.5 μL γ-^{32}p-ATP, and 1 μg GST-MEK1 or MKK6/MKK3 (EMD Millipore, 14–304) recombinant proteins, respectively (58). After adding sodium dodecyl sulfate (SDS) loading buffer, the samples were boiled for 5 min at 100 °C and subjected to SDS polyacrylamide gel electrophoresis.

Glycolysis assays. ECAR was measured by using an XF96 extracellular flux analyzer (Seahorse Bioscience) as previously described (59). In brief, BMDMs were seeded in XF96 microplates. The next day, the cells were either untreated or treated for 3 h with Pam3CSK4 in a nonbuffered assay medium (Seahorse Biosciences). After incubation for 30 min in an incubator without CO_2, the cells were subjected to glycolysis assays with an XF glycolysis stress test kit (Seahorse Biosciences) to measure background noise level (without glucose), basal ECAR (after injection with glucose), and maximal ECAR (after injection with oligomycin).

Statistical Analysis. Statistical analysis was performed using Prism software (GraphPad Software 8.0). Two-way ANOVA with Tukey's multiple comparisons test was used for grouped analysis. Significant changes between two groups were analyzed with two-tailed unpaired *t* test. Kaplan-Meier analyses were performed and the log-rank Mantel-Cox test was employed to determine any statistical difference between the survival curves of two groups. *P* values < 0.05 were considered significant, and the level of significance was indicated as $*P < 0.05$, $**P < 0.01$, $***P < 0.001$, and $****P < 0.0001$. All data are presented as mean ± SD.

Data Availability. All study data are included in the article and/or *SI Appendix*.

ACKNOWLEDGMENTS. This work was supported by a grant from the NIH (AI057555). This study also used the NIH/National Cancer Institute–supported resources under Award No. P30CA016672 at The MD Anderson Cancer Center. T.G. was a visiting student supported by a scholarship from the China Scholarship Council with Grant No. 201906380080.

1. C. Nathan, A. Ding, Nonresolving inflammation. *Cell* **140**, 871–882 (2010).
2. M. F. Neurath, Cytokines in inflammatory bowel disease. *Nat. Rev. Immunol.* **14**, 329–342 (2014).
3. J. S. Yudkin, M. Kumari, S. E. Humphries, V. Mohamed-Ali, Inflammation, obesity, stress and coronary heart disease: Is interleukin-6 the link? *Atherosclerosis* **148**, 209–214 (2000).
4. G. S. Hotamisligil, P. Arner, J. F. Caro, R. L. Atkinson, B. M. Spiegelman, Increased adipose tissue expression of tumor necrosis factor-alpha in human obesity and insulin resistance. *J. Clin. Invest.* **95**, 2409–2415 (1995).
5. O. Nov *et al.*, Interleukin-1β regulates fat-liver crosstalk in obesity by auto-paracrine modulation of adipose tissue inflammation and expandability. *PLoS One* **8**, e53626 (2013).
6. P. Libby, P. M. Ridker, A. Maseri, Inflammation and atherosclerosis. *Circulation* **105**, 1135–1143 (2002).
7. L. M. Coussens, Z. Werb, Inflammation and cancer. *Nature* **420**, 860–867 (2002).
8. A. Wree, L. Broderick, A. Canbay, H. M. Hoffman, A. E. Feldstein, From NAFLD to NASH to cirrhosis-new insights into disease mechanisms. *Nat. Rev. Gastroenterol. Hepatol.* **10**, 627–636 (2013).
9. A. C. Sheka *et al.*, Nonalcoholic steatohepatitis: A review. *JAMA* **323**, 1175–1183 (2020).
10. H. El-Gabalawy, L. C. Guenther, C. N. Bernstein, Epidemiology of immune-mediated inflammatory diseases: Incidence, prevalence, natural history, and comorbidities. *J. Rheumatol. Suppl.* **85**, 2–10 (2010).
11. R. Pahwa, A. Goyal, P. Bansal, I. Jialal, "Chronic inflammation" in *StatPearls* (StatPearls, Treasure Island, 2021).
12. S. P. Weisberg *et al.*, Obesity is associated with macrophage accumulation in adipose tissue. *J. Clin. Invest.* **112**, 1796–1808 (2003).
13. E. Galkina, K. Ley, Immune and inflammatory mechanisms of atherosclerosis (*). *Annu. Rev. Immunol.* **27**, 165–197 (2009).
14. Y. R. Na, M. Stakenborg, S. H. Seok, G. Matteoli, Macrophages in intestinal inflammation and resolution: A potential therapeutic target in IBD. *Nat. Rev. Gastroenterol. Hepatol.* **16**, 531–543 (2019).
15. D. E. Lackey, J. M. Olefsky, Regulation of metabolism by the innate immune system. *Nat. Rev. Endocrinol.* **12**, 15–28 (2016).
16. K. N. Couper, D. G. Blount, E. M. Riley, IL-10: The master regulator of immunity to infection. *J. Immunol.* **180**, 5771–5777 (2008).

17. C. D. Mills, K. Kincaid, J. M. Alt, M. J. Heilman, A. M. Hill, M-1/M-2 macrophages and the Th1/Th2 paradigm. *J. Immunol.* **164**, 6166–6173 (2000).
18. C. D. Mills, M1 and M2 macrophages: Oracles of health and disease. *Crit. Rev. Immunol.* **32**, 463–488 (2012).
19. S. Akira, K. Takeda, Toll-like receptor signalling. *Nat. Rev. Immunol.* **4**, 499–511 (2004).
20. C. Dong, R. J. Davis, R. A. Flavell, MAP kinases in the immune response. *Annu. Rev. Immunol.* **20**, 55–72 (2002).
21. N. Silverman, T. Maniatis, NF-kappaB signaling pathways in mammalian and insect innate immunity. *Genes Dev.* **15**, 2321–2342 (2001).
22. J. Palomo, D. Dietrich, P. Martin, G. Palmer, C. Gabay, The interleukin (IL)-1 cytokine family–Balance between agonists and antagonists in inflammatory diseases. *Cytokine* **76**, 25–37 (2015).
23. S. Siebert, A. Tsoukas, J. Robertson, I. McInnes, Cytokines as therapeutic targets in rheumatoid arthritis and other inflammatory diseases. *Pharmacol. Rev.* **67**, 280–309 (2015).
24. A. Nemetz *et al.*, IL1B gene polymorphisms influence the course and severity of inflammatory bowel disease. *Immunogenetics* **49**, 527–531 (1999).
25. D. B. Ballak, R. Stienstra, C. J. Tack, C. A. Dinarello, J. A. van Diepen, IL-1 family members in the pathogenesis and treatment of metabolic disease: Focus on adipose tissue inflammation and insulin resistance. *Cytokine* **75**, 280–290 (2015).
26. K. Rajamäki *et al.*, Cholesterol crystals activate the NLRP3 inflammasome in human macrophages: A novel link between cholesterol metabolism and inflammation. *PLoS One* **5**, e11765 (2010).
27. C. A. Dinarello, A. Simon, J. W. van der Meer, Treating inflammation by blocking interleukin-1 in a broad spectrum of diseases. *Nat. Rev. Drug Discov.* **11**, 633–652 (2012).
28. J. Hiscott, Triggering the innate antiviral response through IRF-3 activation. *J. Biol. Chem.* **282**, 15325–15329 (2007).
29. K. Clark, L. Plater, M. Peggie, P. Cohen, Use of the pharmacological inhibitor BX795 to study the regulation and physiological roles of TBK1 and IkappaB kinase epsilon: A distinct upstream kinase mediates Ser-172 phosphorylation and activation. *J. Biol. Chem.* **284**, 14136–14146 (2009).
30. J. Jin *et al.*, The kinase TBK1 controls IgA class switching by negatively regulating noncanonical NF-κB signaling. *Nat. Immunol.* **13**, 1101–1109 (2012).
31. J. Yu *et al.*, Regulation of T-cell activation and migration by the kinase TBK1 during neuroinflammation. *Nat. Commun.* **6**, 6074 (2015).
32. Y. Xiao *et al.*, The kinase TBK1 functions in dendritic cells to regulate T cell homeostasis, autoimmunity, and antitumor immunity. *J. Exp. Med.* **214**, 1493–1507 (2017).
33. A. Sorisky, A. S. Molgat, A. Gagnon, Macrophage-induced adipose tissue dysfunction and the preadipocyte: Should I stay (and differentiate) or should I go? *Adv. Nutr.* **4**, 67–75 (2013).
34. H. Kitade, G. Chen, Y. Ni, T. Ota, Nonalcoholic fatty liver disease and insulin resistance: New insights and potential new treatments. *Nutrients* **9**, 387 (2017).
35. C. L. Abram, G. L. Roberge, Y. Hu, C. A. Lowell, Comparative analysis of the efficiency and specificity of myeloid-Cre deleting strains using ROSA-EYFP reporter mice. *J. Immunol. Methods* **408**, 89–100 (2014).
36. J. Branger *et al.*, Anti-inflammatory effects of a p38 mitogen-activated protein kinase inhibitor during human endotoxemia. *J. Immunol.* **168**, 4070–4077 (2002).
37. A. Viola, F. Munari, R. Sánchez-Rodríguez, T. Scolaro, A. Castegna, The metabolic signature of macrophage responses. *Front. Immunol.* **10**, 1462 (2019).
38. B. Everts *et al.*, TLR-driven early glycolytic reprogramming via the kinases TBK1-IKKε supports the anabolic demands of dendritic cell activation. *Nat. Immunol.* **15**, 323–332 (2014).
39. Y. Tan, J. C. Kagan, Innate immune signaling organelles display natural and programmable signaling flexibility. *Cell* **177**, 384–398.e11 (2019).
40. B. Chassaing, J. D. Aitken, M. Malleshappa, M. Vijay-Kumar, Dextran sulfate sodium (DSS)-induced colitis in mice. *Curr. Protoc. Immunol.* **104**, Unit 15, 25 (2014).
41. R. Monteiro, I. Azevedo, Chronic inflammation in obesity and the metabolic syndrome. *Mediators Inflamm.* **2010**, 289645 (2010).
42. C. R. Kahn, G. Wang, K. Y. Lee, Altered adipose tissue and adipocyte function in the pathogenesis of metabolic syndrome. *J. Clin. Invest.* **129**, 3990–4000 (2019).
43. T. Mau, R. Yung, Adipose tissue inflammation in aging. *Exp. Gerontol.* **105**, 27–31 (2018).
44. A. K. Palmer, J. L. Kirkland, Aging and adipose tissue: Potential interventions for diabetes and regenerative medicine. *Exp. Gerontol.* **86**, 97–105 (2016).
45. I. Wernstedt Asterholm *et al.*, Adipocyte inflammation is essential for healthy adipose tissue expansion and remodeling. *Cell Metab.* **20**, 103–118 (2014).
46. S. Schuster, D. Cabrera, M. Arrese, A. E. Feldstein, Triggering and resolution of inflammation in NASH. *Nat. Rev. Gastroenterol. Hepatol.* **15**, 349–364 (2018).
47. K. Kazankov *et al.*, The role of macrophages in nonalcoholic fatty liver disease and nonalcoholic steatohepatitis. *Nat. Rev. Gastroenterol. Hepatol.* **16**, 145–159 (2019).
48. S. Sato *et al.*, Essential function for the kinase TAK1 in innate and adaptive immune responses. *Nat. Immunol.* **6**, 1087–1095 (2005).
49. K. Bandow *et al.*, LPS-induced chemokine expression in both MyD88-dependent and -independent manners is regulated by Cot/Tpl2-ERK axis in macrophages. *FEBS Lett.* **586**, 1540–1546 (2012).
50. C. D. Dumitru *et al.*, TNF-alpha induction by LPS is regulated posttranscriptionally via a Tpl2/ERK-dependent pathway. *Cell* **103**, 1071–1083 (2000).
51. K. Senger *et al.*, The kinase TPL2 activates ERK and p38 signaling to promote neutrophilic inflammation. *Sci. Signal.* **10**, eaah4273 (2017).
52. K. Clark *et al.*, Novel cross-talk within the IKK family controls innate immunity. *Biochem. J.* **434**, 93–104 (2011).
53. P. Zhao *et al.*, TBK1 at the crossroads of inflammation and energy homeostasis in adipose tissue. *Cell* **172**, 731–743.e12 (2018).
54. Y. Li *et al.*, NIK links inflammation to hepatic steatosis by suppressing PPARα in alcoholic liver disease. *Theranostics* **10**, 3579–3593 (2020).
55. W. W. Reiley *et al.*, Deubiquitinating enzyme CYLD negatively regulates the ubiquitin-dependent kinase Tak1 and prevents abnormal T cell responses. *J. Exp. Med.* **204**, 1475–1485 (2007).
56. E. Schreiber, P. Matthias, M. M. Müller, W. Schaffner, Rapid detection of octamer binding proteins with 'mini-extracts', prepared from a small number of cells. *Nucleic Acids Res.* **17**, 6419 (1989).
57. G. Xiao, E. W. Harhaj, S. C. Sun, NF-kappaB-inducing kinase regulates the processing of NF-kappaB2 p100. *Mol. Cell* **7**, 401–409 (2001).
58. M. R. Waterfield, M. Zhang, L. P. Norman, S. C. Sun, NF-kappaB1/p105 regulates lipopolysaccharide-stimulated MAP kinase signaling by governing the stability and function of the Tpl2 kinase. *Mol. Cell* **11**, 685–694 (2003).
59. X. Zhou *et al.*, The deubiquitinase Otub1 controls the activation of $CD8^+$ T cells and NK cells by regulating IL-15-mediated priming. *Nat. Immunol.* **20**, 879–889 (2019).